Electronic Supplementary Material (ESI) for Materials Horizons.

Supporting Information for

Layered Polymer Composite Foams for Broadband Ultra-Low Reflectance EMI Shielding: A Computationally Guided Fabrication Approach

Li Ma [a], *Linfeng Wei* [a], *Mahdi Hamidinejad* [b]*, *and Chul B. Park* [a]*

[a] Department of Mechanical and Industrial Engineering, University of Toronto, 5 King's College Road, Toronto, Ontario M5S 3G8, Canada

[b] Department of Mechanical Engineering, University of Alberta, 9211-116 Street NW, Edmonton, AB T6G1H9, Canada

* Corresponding Authors: park@mie.utoronto.ca, +1 416-978-3053
mahdi.hamidi@ualberta.ca,

Preparation of $Ti_3C_2T_x$ MXene Nanosheets

In this study, a method for the synthesis of few-layered Ti3C2Tx nanosheets via the etching of Ti_3AlC_2 powder using a LiF/HCl solution is described. Initially, 4 g of LiF powder was dissolved into 50 ml hydrochloric acid (9N) under continuous stirring at 45℃. Subsequently, 2.5 g of Ti_3AlC_2 powder was gradually added to the LiF/HCl solution under continuous stirring. After 24 hours of stirring at 40℃, the resulting acidic mixture was washed with DI water via centrifugation (4,000 rpm for 5 mins) for several cycles until the solution pH value was above 6.

The sediment of MXene in DI water was then sonicated for 5 mins and centrifuged at 3,500 rpm for 5 min to yield a dark green colloidal suspension containing few-layered

$Ti_3C_2T_x$ nanosheets.[1] This colloidal suspension was carefully collected, and vacuum filtered into MXene films for the later preparation of SiCnw/MXene heterostructures.

Preparation of PDDA-modified SiCnw

A total of 1 g of SiCnw was slowly added into a 250 mL solution with 0.4 wt% PDDA while continuously stirring for 6 hours. Subsequently, the modified SiCnw was collected via centrifugation and subjected to five rounds of washing with deionized water. The resulting modified SiCnw possessed a positive zeta potential and was dried overnight in a vacuum oven.[2]

Fabrication of PVDF/SiCnw@MXene nanocomposites

In this work, PVDF/30 wt% SiCnw@MXene10:1 composite was fabricated via solvent casting. 0.078 g of Ti3C2Tx MXene was dispersed in 50 mL of deionized water and subjected to 30 minutes of sonication under an argon atmosphere. Following this, 0.78 g of modified SiCnw was added to the mixture, which was then sonicated for 15 minutes under an argon environment, followed by 30 minutes of continuous stirring. The SiCnw and MXene nanosheets self-assembled via electrostatic forces, with a SiCnw: MXene weight ratio of 10:1. The resulting SiCnw/MXene hybrid was collected by centrifugation, then dispersed in 25 mL of DMF solution and sonicated for 15 minutes.

Subsequently, following the schematic representation in Figure S1(a), 2 g of PVDF pellets were dissolved and dispersed in the hybrid solution with continuous stirring for 3 hours at 80°C. The PVDF/SiCnw@MXene composite was obtained via quick phase inversion after injecting the

mixture into a water tank. To ensure a homogeneous distribution of SiCnw@MXene nanofillers within the PVDF matrix, the resulting PVDF composite was rapidly cooled in liquid nitrogen and subsequently ground into a fine powder. The resulting powder was then subjected to hot-pressing, where it was compressed under controlled temperature and pressure conditions. This hot-pressing step transformed the powder into a compact rectangular shape, measuring 7.9 mm × 15.8 mm × 1.8 mm.

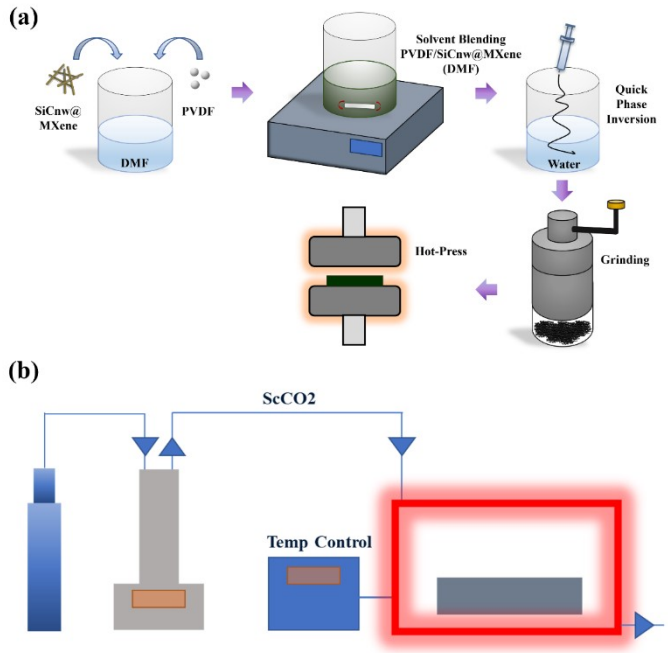

Figure S1. Schematic of the (a) fabrication of PVDF/SiCnw@MXene composite (b) batch foaming process.

Fabrication of PVDF/CNT composites

A composite of PVDF and 8 wt% CNT was fabricated via solvent casting. 0.174 g of CNT was initially dispersed in 25 mL of DMF and sonicated for 30 minutes. Next, 2 g of PVDF pellets were dissolved and dispersed in the DMF solution, subjected to continuous stirring at 80°C for 3 hours. The resulting PVDF/CNT mixture was obtained via quick phase inversion upon injection

into a water tank. Subsequently, the resultant PVDF composite was quenched in liquid nitrogen, ground into powder, and hot-pressed into a rectangular shape measuring 7.9 mm × 15.8 mm × 1.8 mm.

Foaming mechanisms

A one-step batch foaming process was employed to create microcellular structures in polyvinylidene fluoride (PVDF) composites, as illustrated in Fig. S1(b). This involved loading the specimen into a high-pressure autoclave filled with a pressurized physical blowing agent (PBA) such as supercritical CO_2 at a designated pressure and temperature. The CO_2 gas molecules dissolved into the polymer matrix, resulting in a homogeneous polymer/gas mixture that was maintained at a constant temperature and saturating pressure for a specified duration. After saturation, phase separation was induced in the polymer/gas mixture through an instant depressurization process, whereby the pressurized CO_2 gas was rapidly exhausted from the system by opening the valve, causing immediate cell nucleation due to significant thermodynamic instability.[3,4] Nucleated cells then began to grow within the viscoelastic polymer melt, and the development of a microcellular structure was stabilized by submerging the chamber into an ice bath to solidify the hot polymer matrix.

		Temperature (°C)	125	126.8	127.5	129.5	130	132.5	133	134.3	136	136.8	137	138	138.5
PVDF composites	30 wt% SiCnw	Void Fraction (%)	~ 40	~ 60		~ 70		~ 80	~ 85						
	30 wt% SiCnw@MXene10:1		~ 25		~ 40		~ 50		~ 60	~ 70				~ 80	
	8 wt% CNT										~ 40	~ 50	~ 60		~ 70
PBA: CO_2; Saturation time: 30mins; Saturation pressure: 2000 Psi															

Table S1. The void fractions of PVDF composite foams with various material compositions and different foaming conditions.

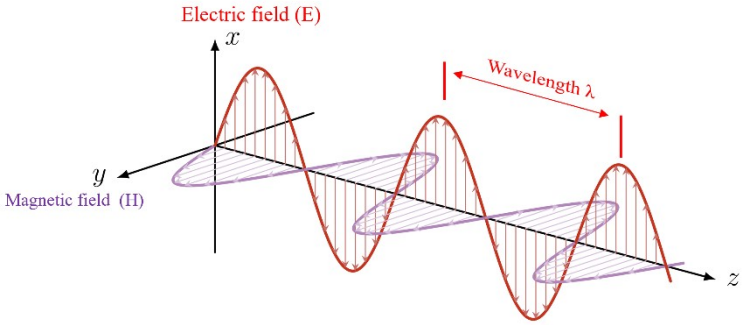

Figure S2. Schematic illustration of propagating EM wave.

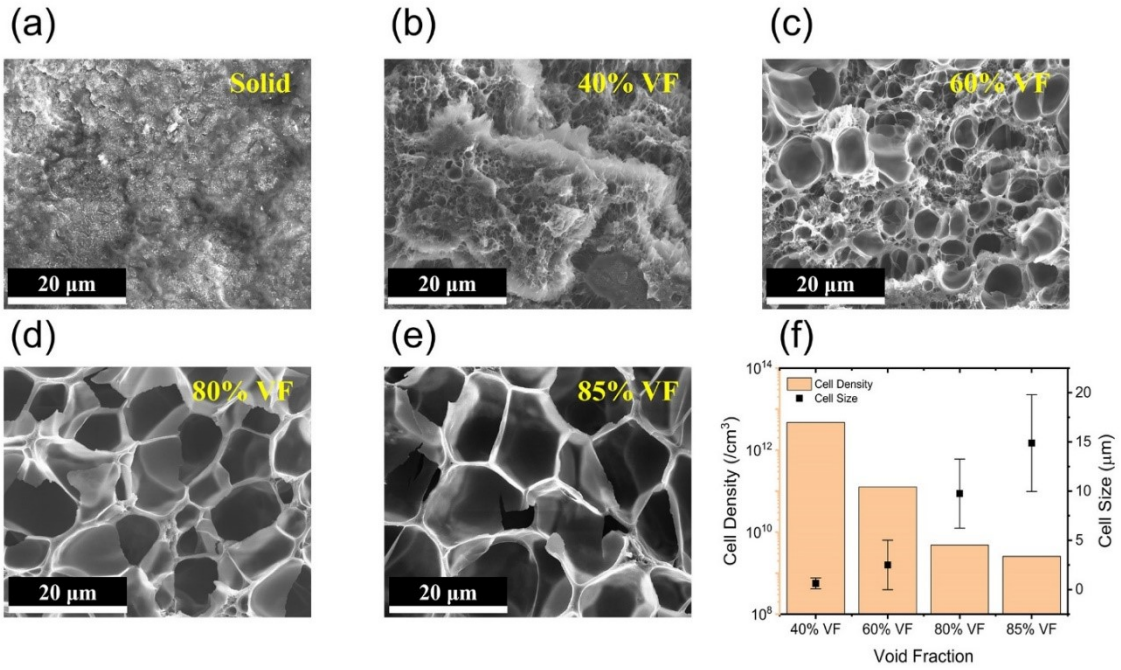

Figure S3. (a-e) SEM images and (f) microstructure parameters of PVDF/8 wt% CNT composite foams with varied void fractions.

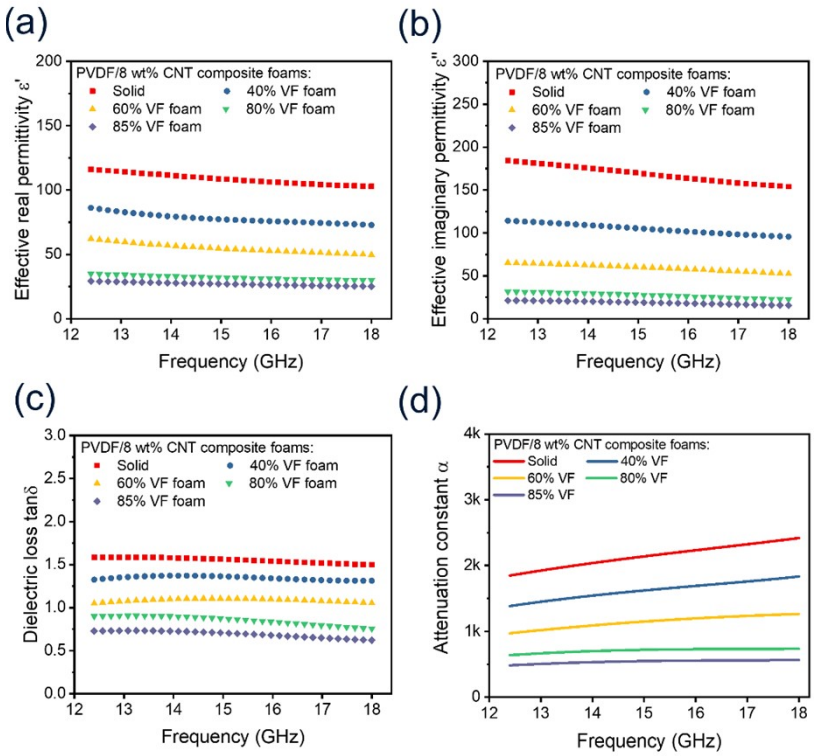

Figure S4. (a) Effective real permittivity; (b) effective imaginary permittivity; (c) tangent dielectric loss ($tan\delta = \frac{\varepsilon''}{\varepsilon'}$); and (d) attenuation constant for PVDF/8 wt% CNT composite foams with varied void fractions.

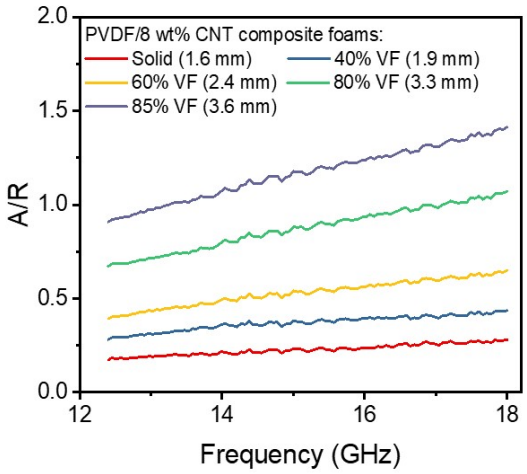

Figure S5. Absorption-to-reflection ratios for PVDF/8 wt% CNT composite foams with varied void fractions and corresponding thicknesses.

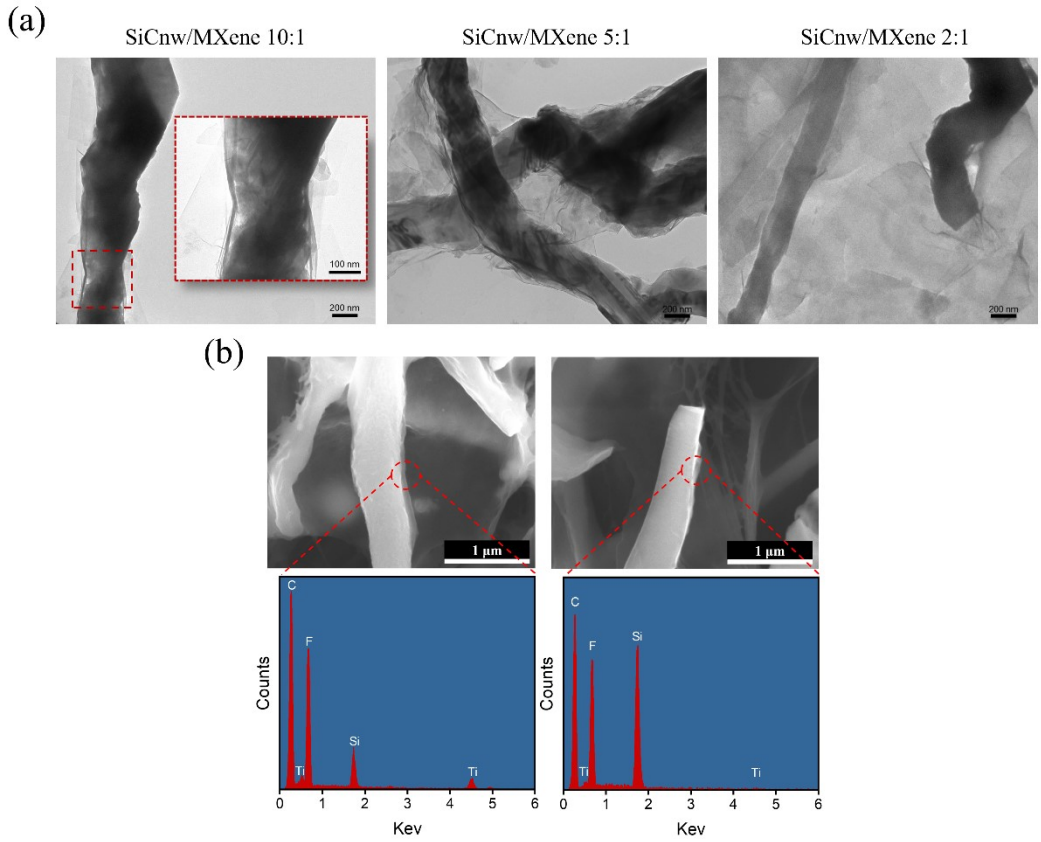

Figure S6. (a) TEM images of SiCnw/MXene hybrids with various filler ratios; (b) Microstructures and corresponding

EDX spectra of SiCnw/MXene hybrids in PVDF composite foams.

As depicted in Fig. S6 (a), with a SiCnw/MXene ratio of 2:1, an excessive loading of MXene led to significant agglomeration, thereby causing a lack of assembly between the SiCnw and MXene nanosheets. In the case of a 5:1 ratio, MXene agglomeration was less severe, but it still indicated suboptimal assembly efficiency between SiCnw and MXene nanosheets. Thus, to maximize the number of heterogeneous interfaces, the hybrid required less MXene and more SiCnw. Moreover, such agglomeration could hinder impedance matching and result in a conduction loss, as per our previous study. Conversely, a ratio of 10:1 demonstrated optimal interfacial engineering, with high SiCnw loading offering additional sites for SiCnw/MXene heterogeneous interfaces. Consequently, a ratio of 10:1 was selected for this study.

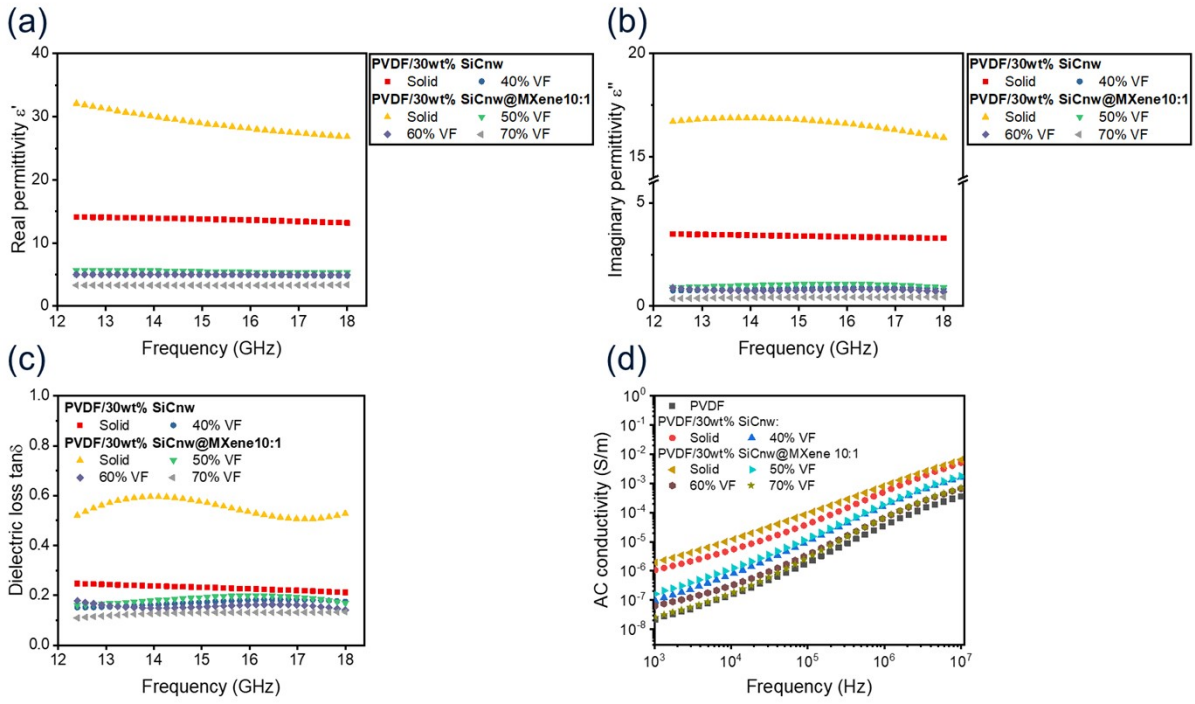

Figure S7. (a) Effective real permittivity; (b) effective imaginary permittivity; (c) tangent dielectric loss ($tan\delta = \frac{\varepsilon''}{\varepsilon'}$); and (d) AC conductivity for PVDF composite foams with varied filler compositions and void fractions.

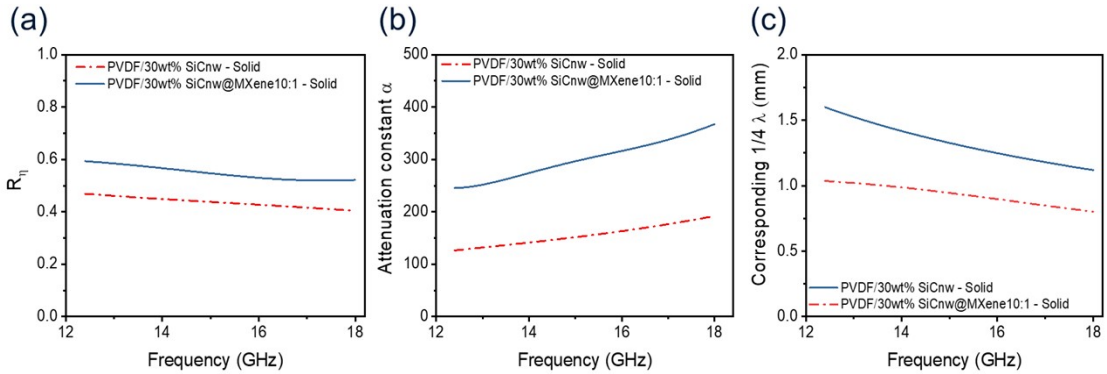

Figure S8. (a) Intrinsic surface reflectivity; (b) attenuation constant; and (c) corresponding quarter wavelength for PVDF/30 wt% SiCnw composite and PVDF/30 wt% SiCnw@MXene10:1 composite.

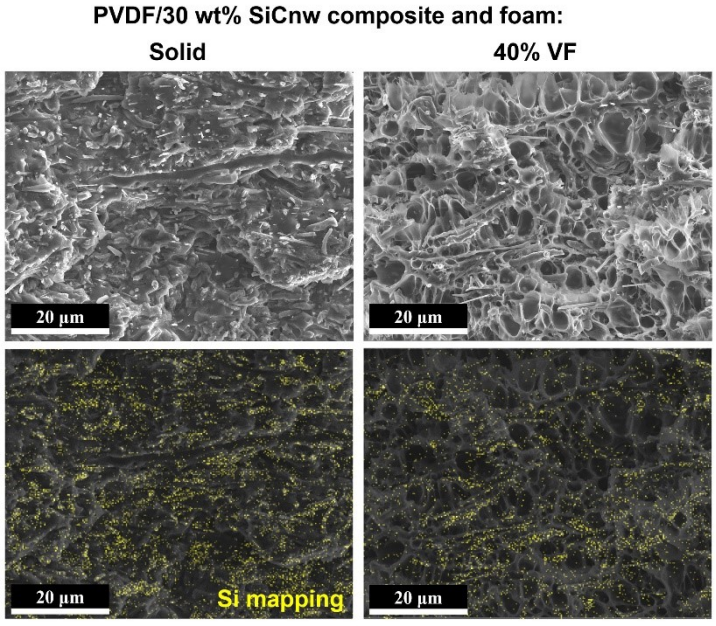

Figure S9. Microstructure images and corresponding Si EDX mapping of PVDF/SiCnw composite and foam.

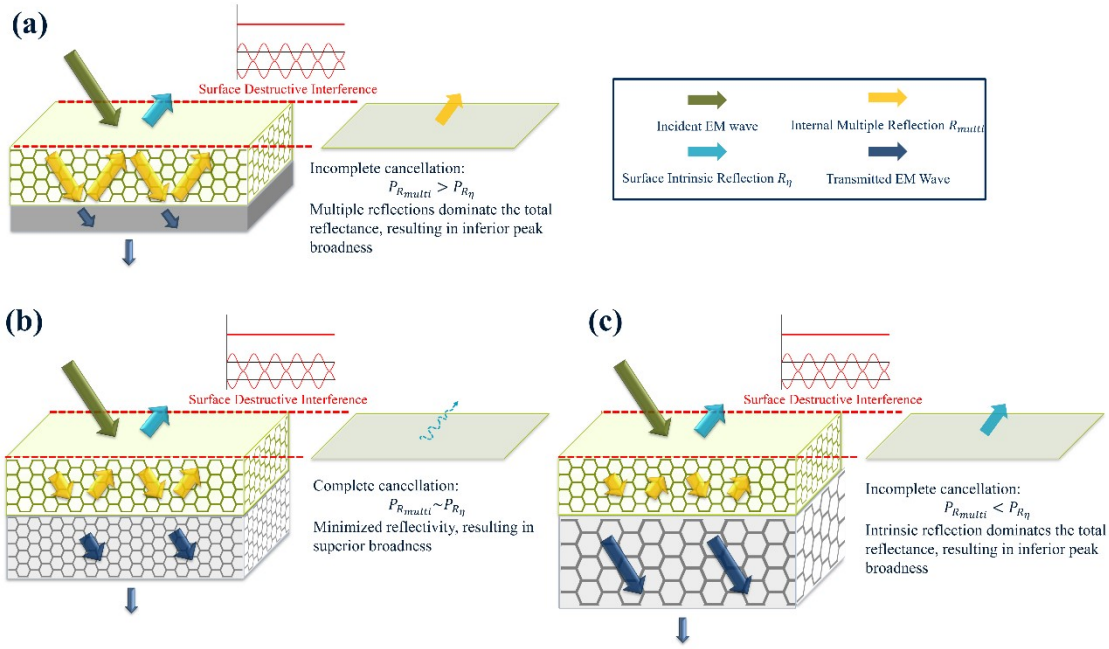

Figure S10. Schematic illustration of input impedance matching and destructive interference between the intrinsic surface reflection and multiple reflections of the absorption layer.

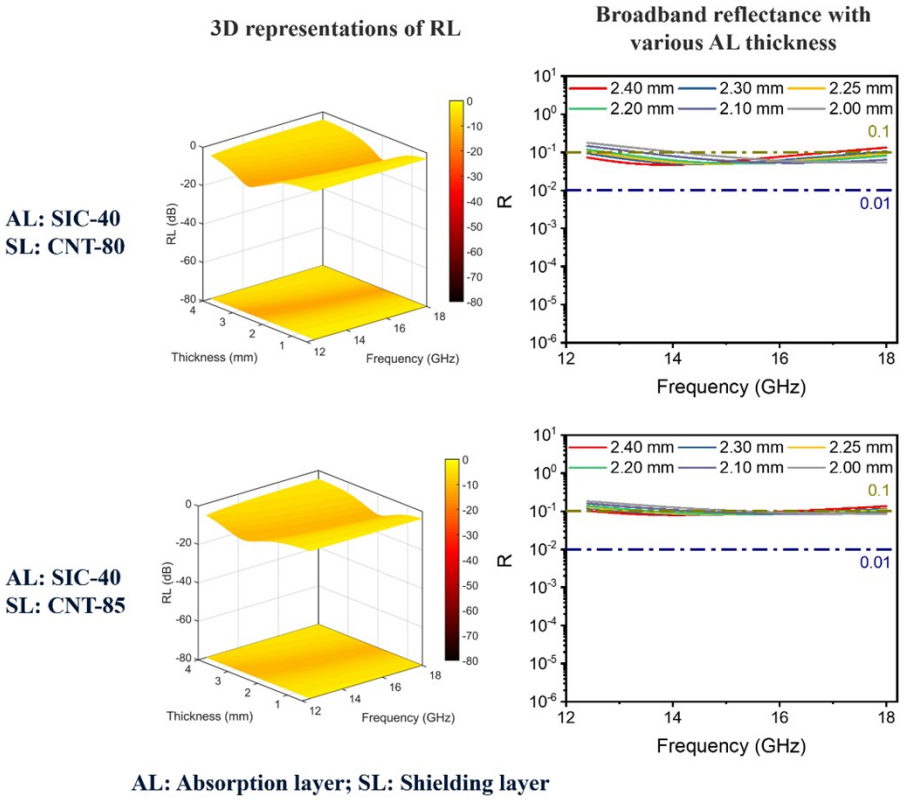

Figure S11. Theoretical computations of broadband R-values with varied absorbent thickness for layered PVDF

nanocomposite foams consisting of SIC-40 as the absorption layer (AL) and varied shielding layers (SL).

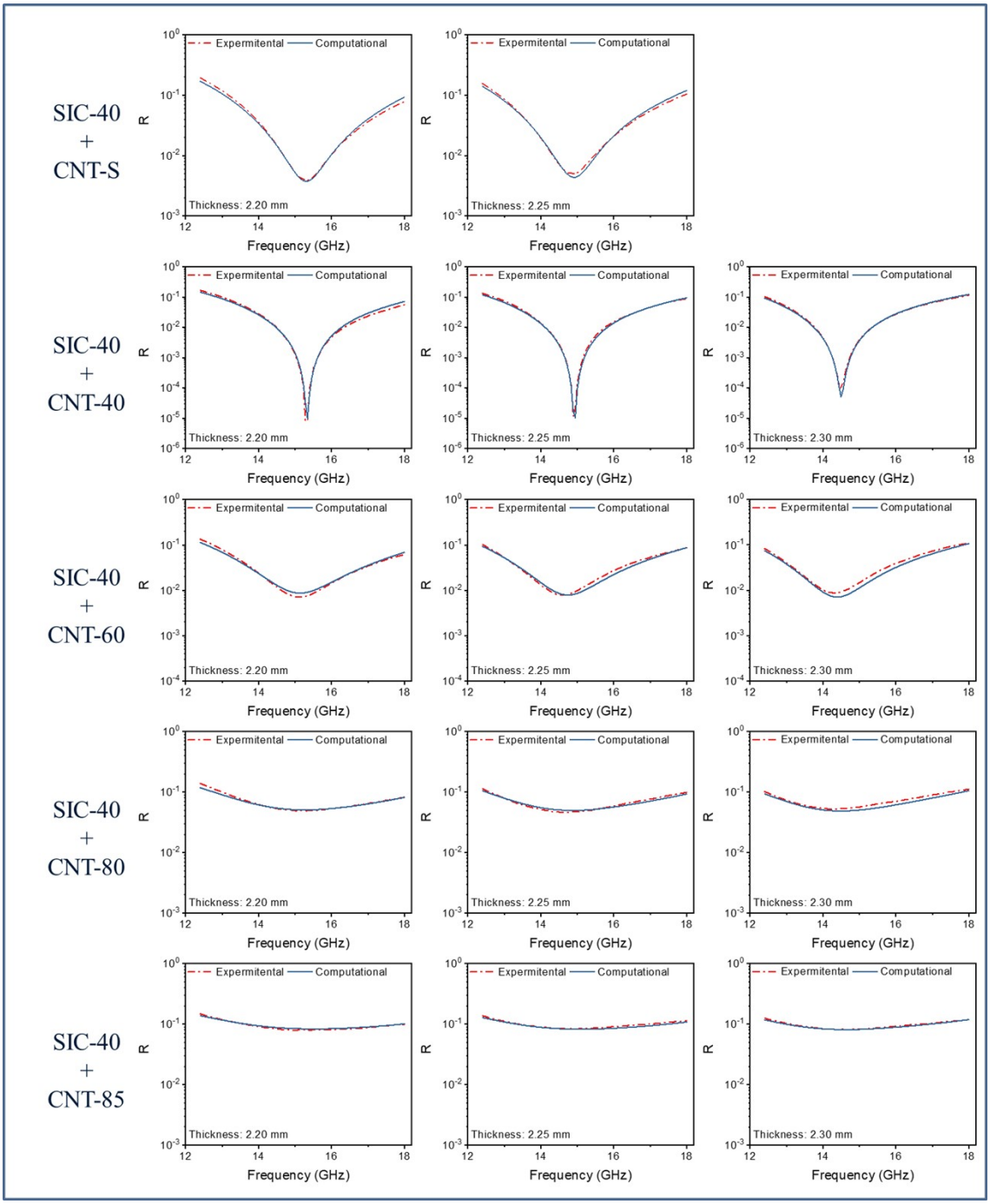

Figure S12. Validation of experimental results and theoretical computations for layered composite foams consisted of SIC-40 as the absorption layer and varied shielding layers.

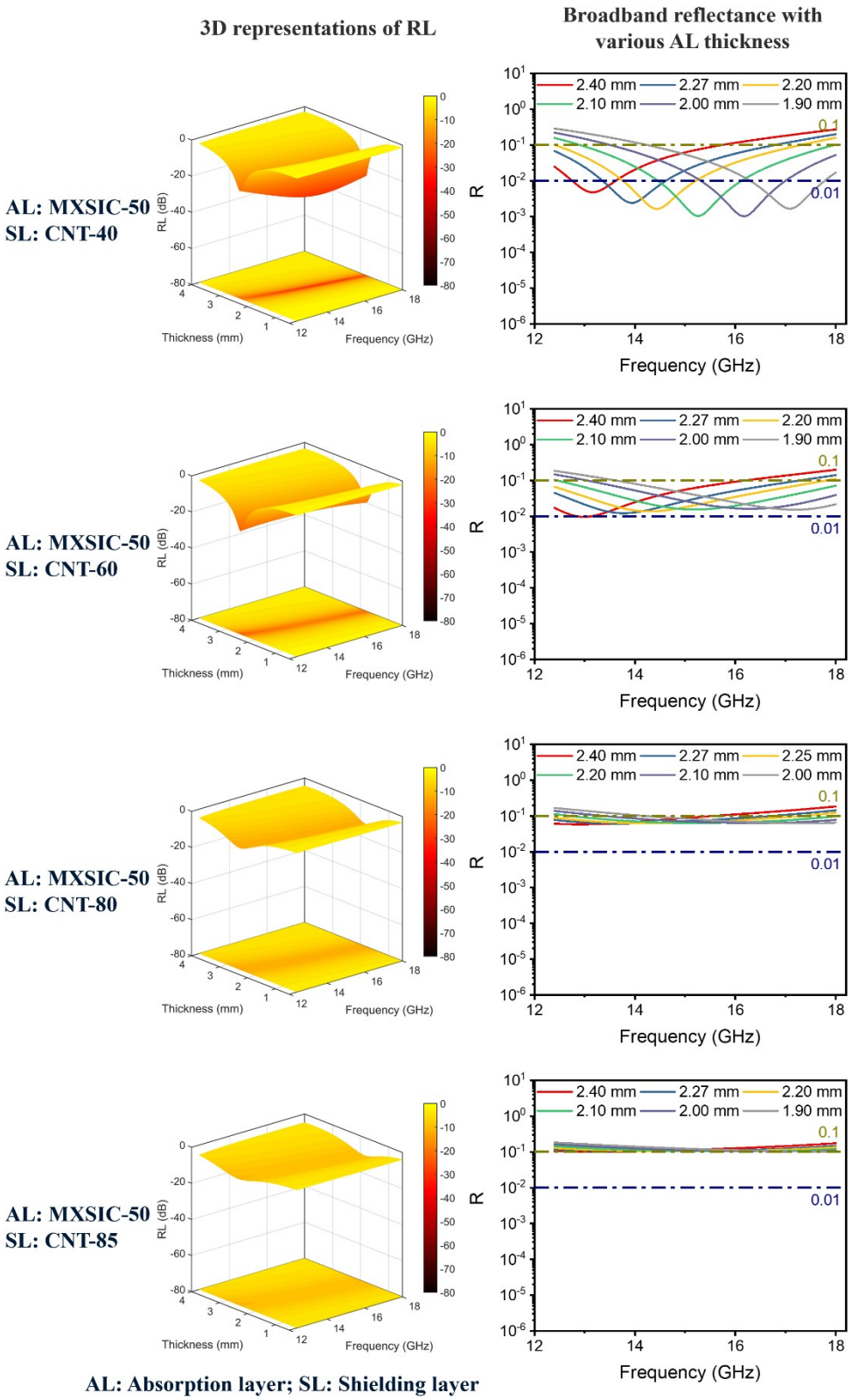

Figure S13. Theoretical computations of broadband R-values with varied absorbent thickness for layered PVDF

nanocomposite foams consisting of MXSIC-50 as the absorption layer (AL) and varied shielding layers (SL).

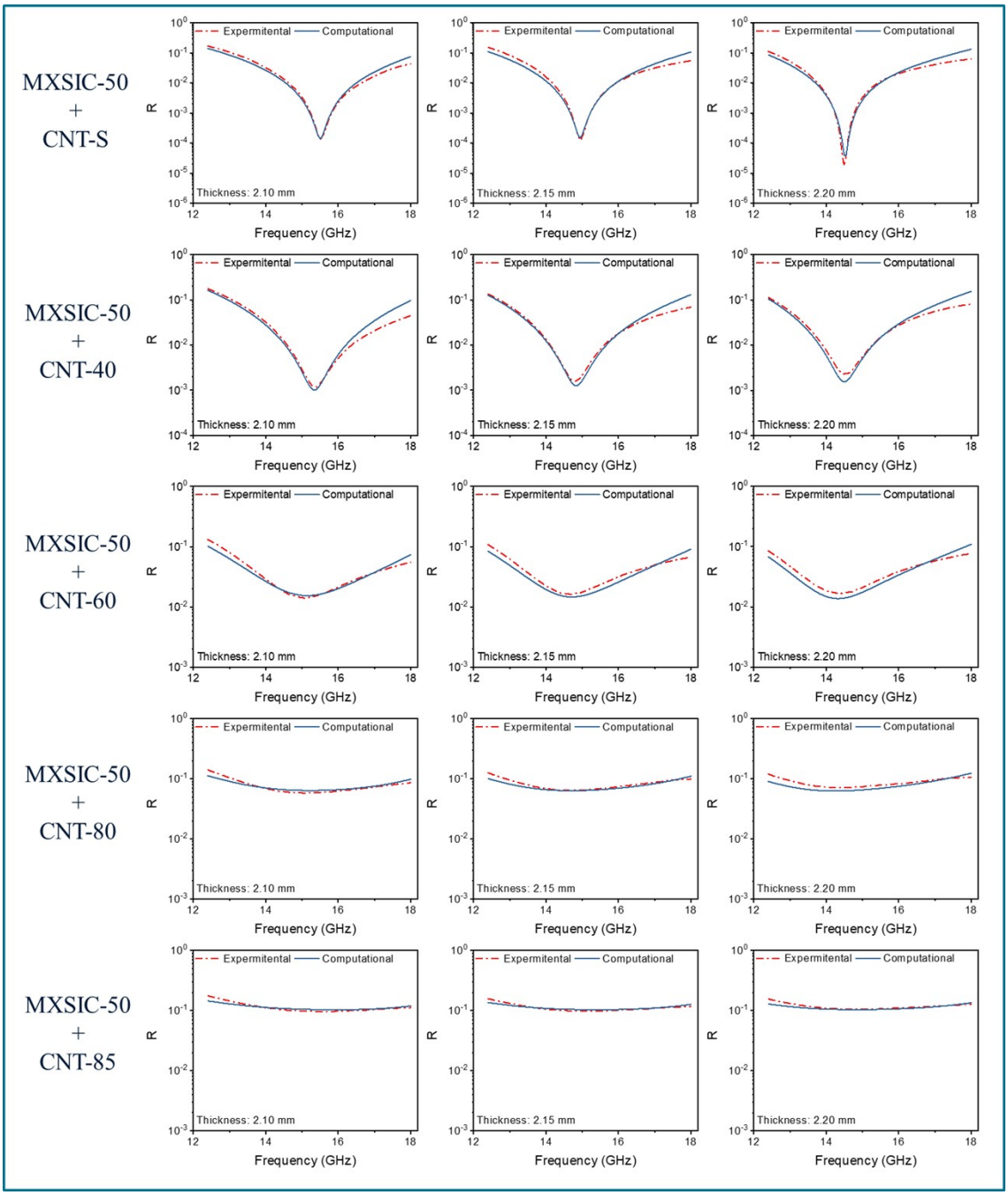

Figure S14. Validation of experimental results and theoretical computations for layered composite foams consisted of MXSIC-50 as the absorption layer and varied shielding layers.

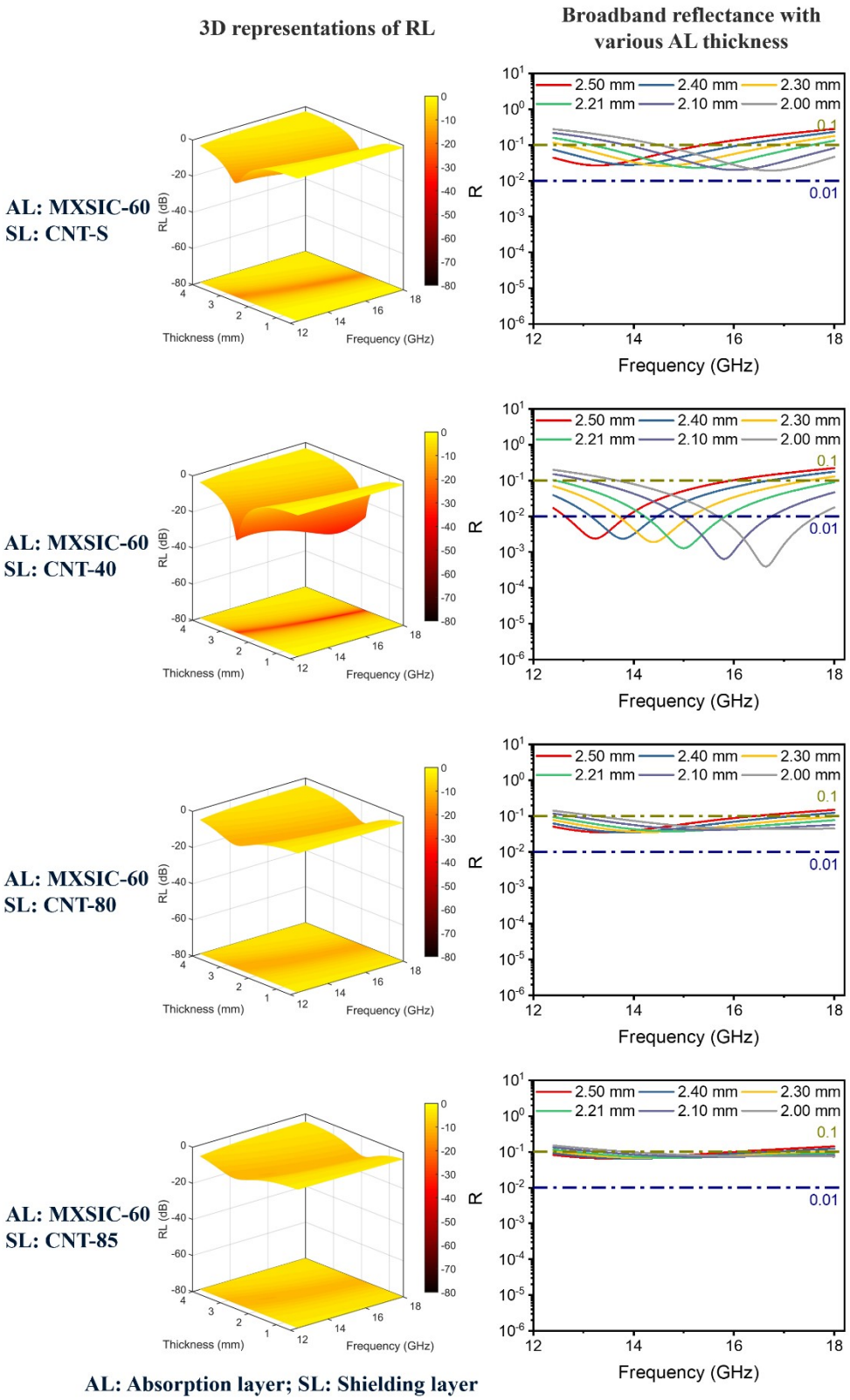

Figure S15. Theoretical computations of broadband R-values with varied absorbent thickness for layered PVDF nanocomposite foams consisting of MXSIC-60 as the absorption layer (AL) and varied shielding layers (SL).

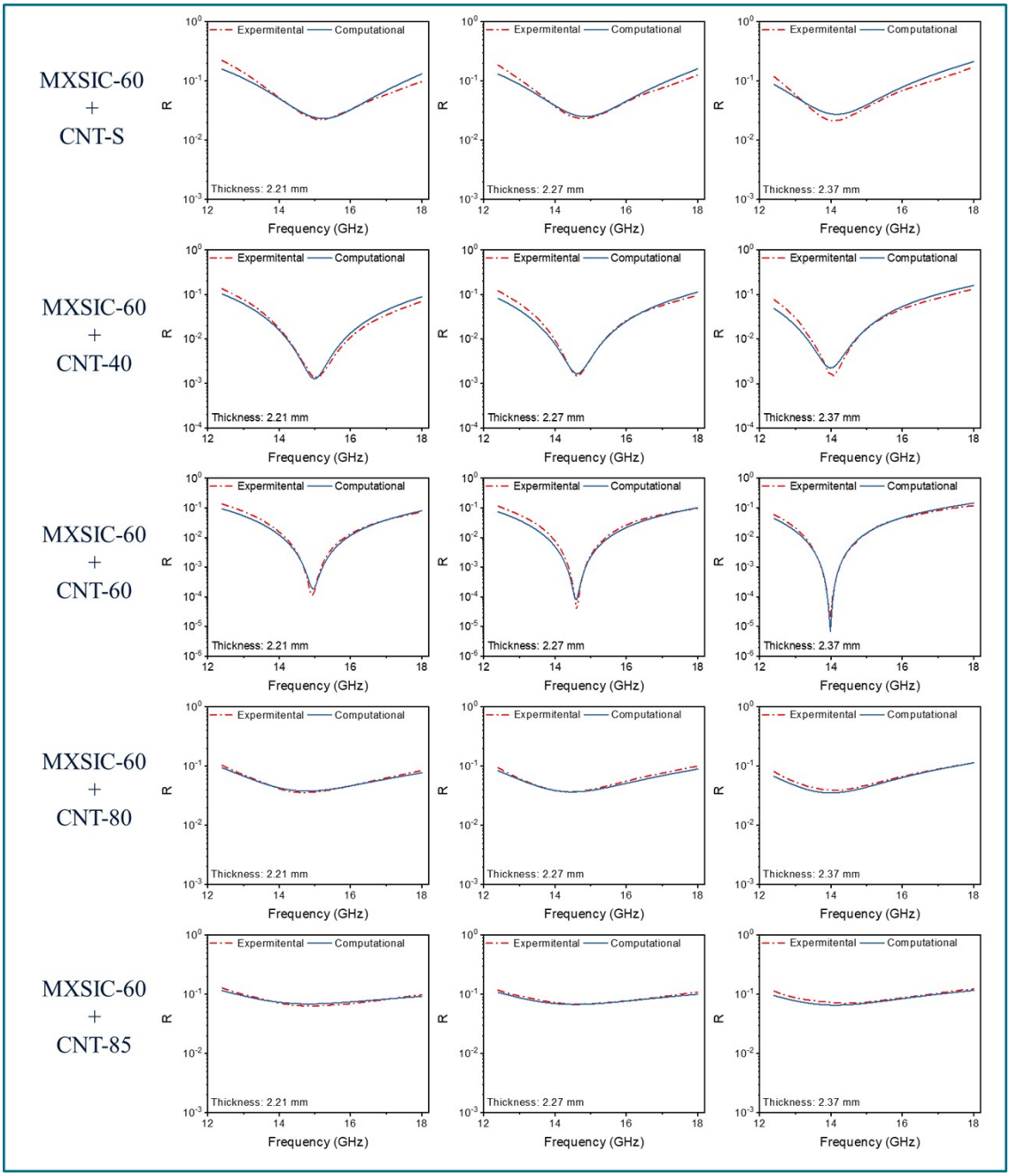

Figure S16. Validation of experimental results and theoretical computations for layered composite foams consisted of MXSIC-60 as the absorption layer and varied shielding layers.

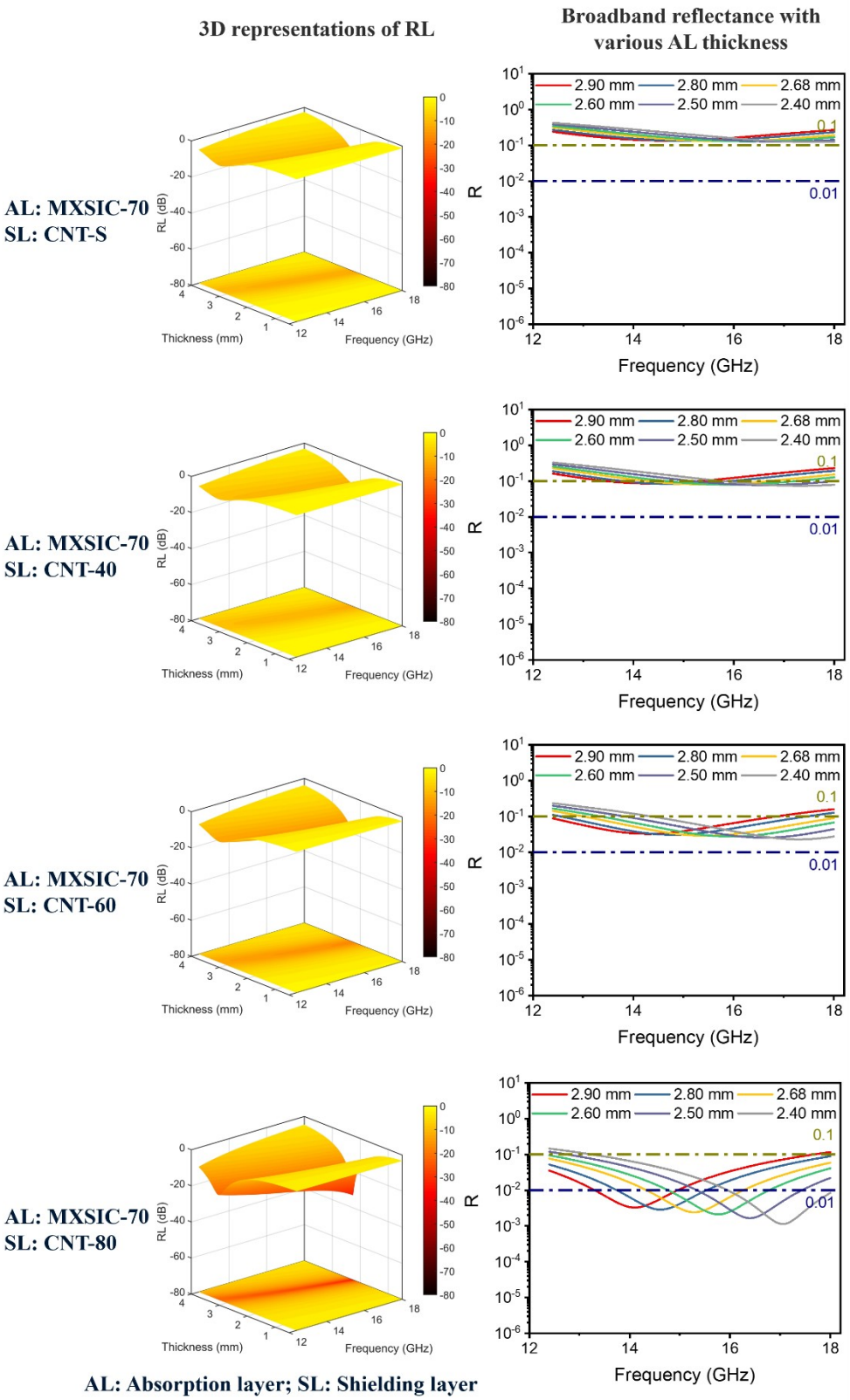

Figure S17. Theoretical computations of broadband R-values with varied absorbent thickness for layered PVDF nanocomposite foams consisting of MXSIC-70 as the absorption layer (AL) and varied shielding layers (SL)

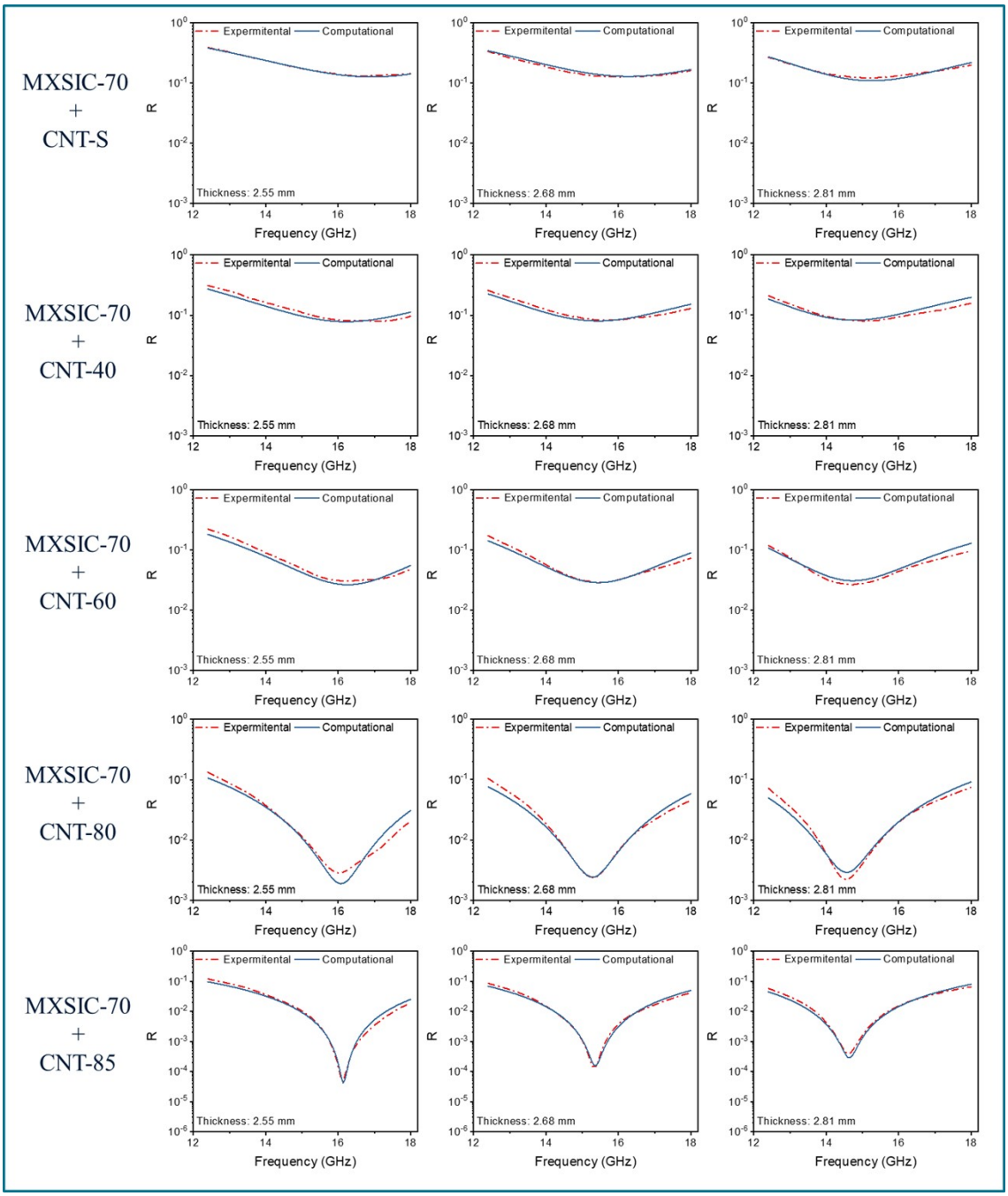

Figure S18. Validation of experimental results and theoretical computations for layered composite foams consisted of MXSIC-70 as the absorption layer and varied shielding layers.

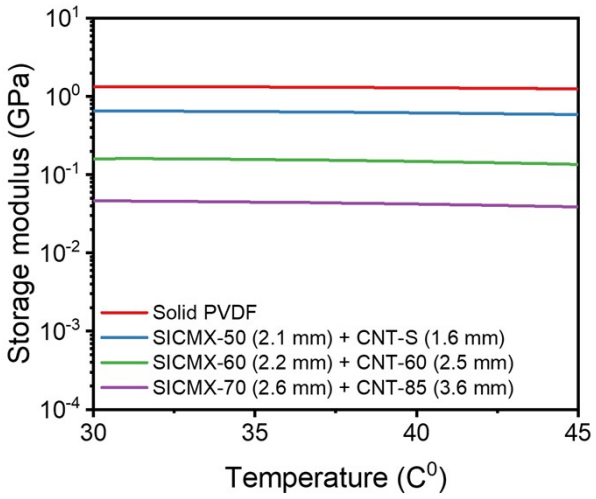

Figure S19. The storage modulus for layered PVDF composite foams with various absorption layers coupled with corresponding input impedance-matched shielding layers, compared to neat PVDF.

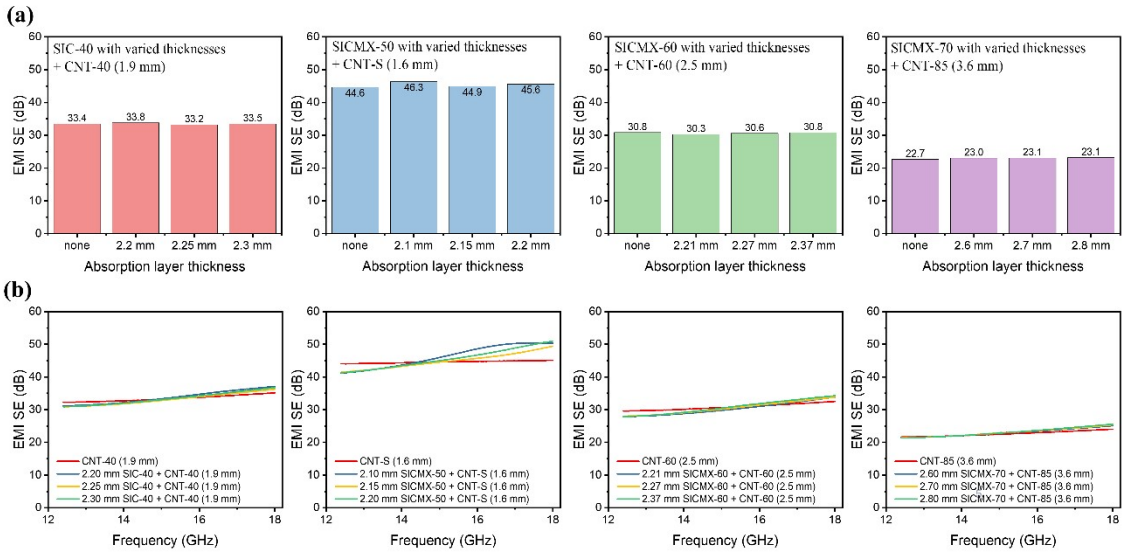

Figure S20 (a) Average EMI SE across difference absorbent thicknesses in layered PVDF composite foams comprising SIC-40, SICMX-50, SICMX-60, and SICMX-70 as absorption layers, with corresponding shielding layers of CNT-S, CNT-40, CNT-60, and CNT-85. (b) Broadband EMI SE corresponded to scenario (a).

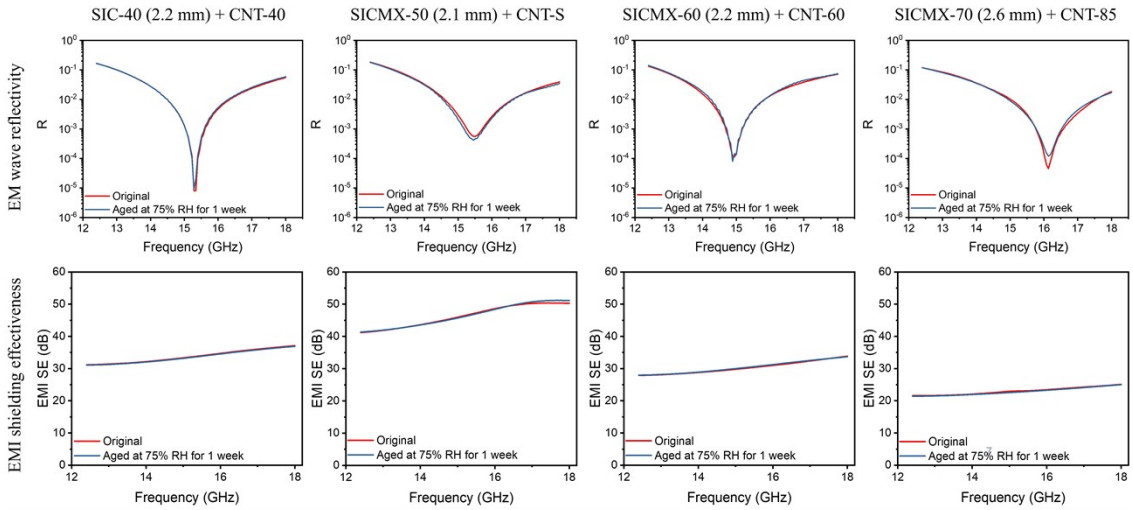

Figure S21. Comparison of EMI shielding performance: layered PVDF composite foams before and after aging at 75% relative humidity for one week

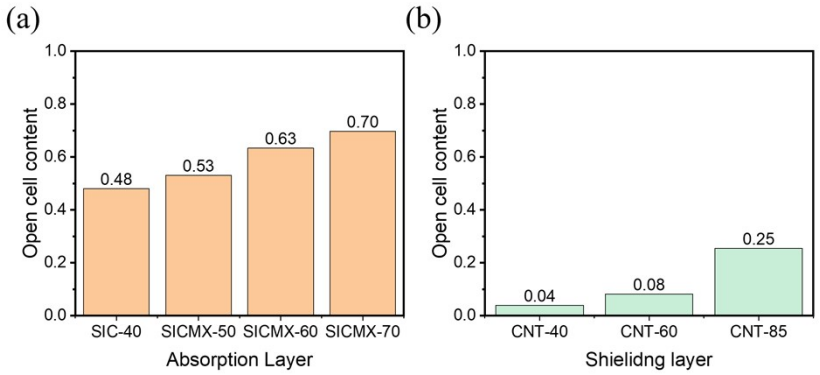

Figure S22. Open cell content in PVDF composite foams: (a) absorption layers and (b) shielding layers

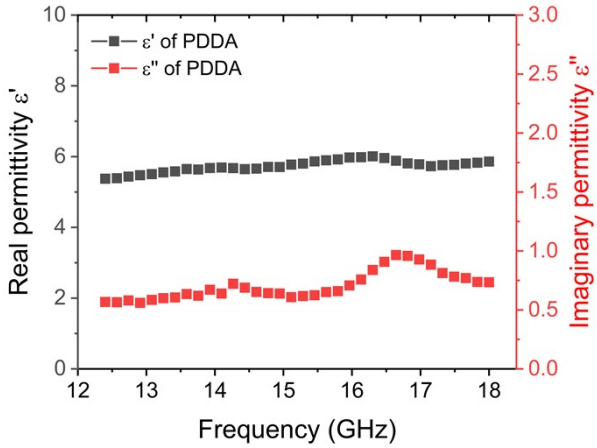

Figure S23. Effective real permittivity and imaginary permittivity of PDDA.

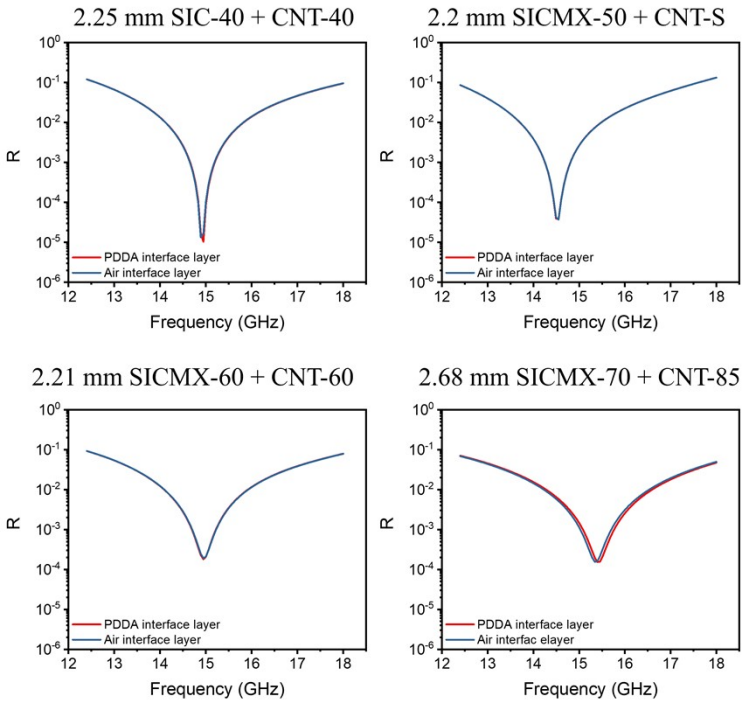

Figure S24. EM wave reflectivity of layered PVDF composite foams with SICMX-50, SICMX-60, and SICMX-70 as absorption layers, coupled with corresponding impedance-matched shielding layers: a comparative theoretical computation between using PDDA and air as interface layers.

Fig. S24 reveals that the existence of a PDDA interface layer has a negligible impact on the reflectivity of the layered PVDF composite foams, relative to an air interface. This is primarily due to the PDDA interface layer's thin thickness, low permittivity, and minimal dielectric loss.

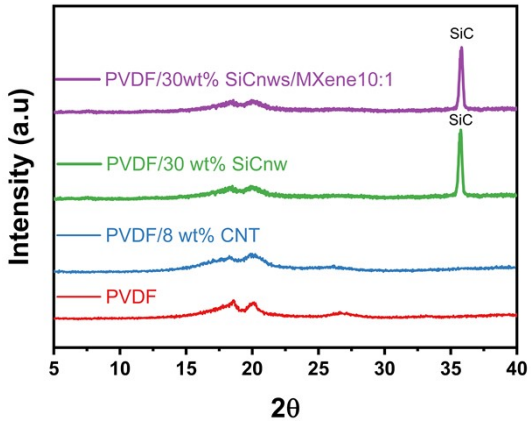

Figure S25. XRD characterizations for PVDF composites with varied material compositions.

Reference:

1 M. Naguib, O. Mashtalir, J. Carle, V. Presser, J. Lu, L. Hultman, Y. Gogotsi and M. W. Barsoum, *ACS Nano*, 2012, **6**, 1322–1331.

2 C. Liang, M. Hamidinejad, L. Ma, Z. Wang and C. B. Park, *Carbon N Y*, 2020, **156**, 58–66.

3 S. N. Leung, A. Wong, Q. Guo, C. B. Park and J. H. Zong, *Chem Eng Sci*, 2009, **64**, 4899–4907.

4 S. N. Leung, C. B. Park, D. Xu, H. Li and R. G. Fenton, *Ind Eng Chem Res*, 2006, **45**, 7823–7831.